SURFACE STRUCTURE STUDY OF IMIDAZOLIUM BASED IONIC LIQUID

by

RAJESH KADEL

A REPORT

submitted in partial fulfillment of the requirements for the degree

MASTER OF SCIENCE

Department of Physics
College of Arts and Sciences

KANSAS STATE UNIVERSITY
Manhattan, Kansas

2008

Approved by:
Major Professor
Bruce Law

Abstract

Interest in the properties of room-temperature ionic liquids is rapidly expanding. Although there have been numerous studies concerning their preparation, their use as a reaction medium and their physical properties, Ionic Liquids (ILs) are so new that many of their bulk physicochemical properties, optical properties, surface properties, toxicities etc. are unknown or only just beginning to be characterized. The highly polar nature of the ILs causes the surfaces of the liquids to become highly ordered in comparison with the surfaces of many other types of organic liquids. Surface structuring at the liquid-vapor interface of the imidazolium based ILs can be examined by using Brewster Angle Ellipsometry and Contact Angle Measurement. The preliminary observation of Ellipsometric measurement shows that there is an interfacial order-disorder transition at temperature T_c=385 K. This result is not analyzed yet but the initial thought behind this is an indication of a ferroelectric transition at the liquid-vapor interface of dipole moment of ILs. From the contact angle measurement it is shown that there is a remarkable change in the contact angle of the imidazolium based ILs over short interval of time (~ ten minutes). Also study of the spreading of the ILs on hard surface shows that there is some definite structural dependence.

Table of Contents

List of Figures

List of Tables

Acknowledgements

I would like to thank my major professor Dr. Bruce Law for the massive amount of time he contributed in the form of guidance and assistance in this project, and for lending words of encouragement when the going got tough (which it did quite often). I would also like to thank the other members of the Law liquid surfaces group, notably Sean McBride, Daniel Frost, Frank male and Eric Stalcup who helped greatly during my research.

CHAPTER 1 – Introduction

Most industrial solvents using these days are organic compounds which are volatile. These compounds have narrow liquid range (~ up to 200^{o}C). So the present solvents are major source of environment pollution. These compounds have been studied for more than hundred years and well characterized. There is an intense research effort to replace volatile organic solvents by new class of solvents called ionic liquids (ILs). These solvents are often fluid at room temperature, so called room-temperature ionic liquids and consist entirely of ionic species-molecular cations and inorganic anions, unlike their inorganic ionic liquid counterparts, such as NaCl, which are liquid at very high temperature~ 800^{o}C and in general very corrosive. ILs posses a number of extremely useful properties: i) they are non-volatile; ii) they have a very large liquidus region in many cases from room temperature up to 300-400^{o}C; iii) their chemical makeup allow them to be readily tailored by changing their organic/inorganic constituents in order to produce liquids with a wide range of useful physicochemical properties. These fascinating properties make ILs of fundamental interest to all scientists. The molecular cation has low degree of symmetry, which reduces the lattice energy of the crystalline form of the salt and hence lowers the melting point (K.R.Sedden, 1998). Properties such as melting point, viscosity, density and hydrophobicity can be varied by simple change to the structure of the ions.

The possible choices of cations and anions that will result in the formation of ILs are numerous. Few of them are shown in fig.1.1. Of course, the most popular ILs are the di-alkyl-imidazolium salts, probably due to their ease of synthesis and

<u>Figure 1.1</u> Structure of different ionic liquids.

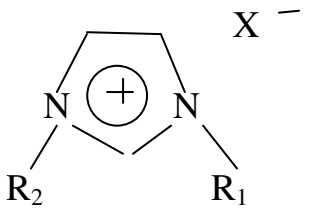

imidazolium

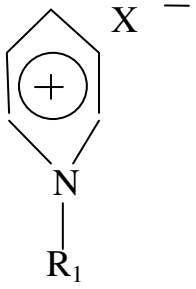

pyridinium

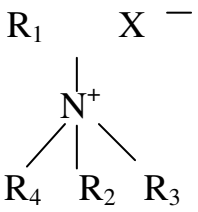

quaternary ammonium

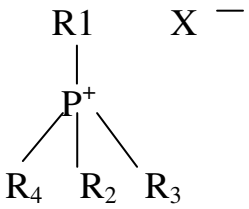

tetra alkyalphosphonium

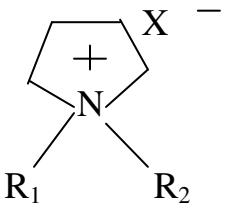

pyrrolidinium

attractive physical properties. The anion (X^-) can be any of variety of species: imidazolium, quaternary, tetra alkyalphosphonium, and pyrrolidinium, including nitrate [NO_3^-], acetate [$CH_3CO_2^-$], trifluoroborate [$CF_3CO_2^-$], tetrafluoroborate [BF_4^-], and hexafluorophosphate [PF_6^-]. The substituents on the cation are typically alkyl chain, but contain any Varity of other functional groups (e.g. fluoroalkyl, alkenyl, methoxy etc.).

As ILs are composed of molecular cations and an inorganic anions, their physico-chemical properties can be tailored by the judicious selection of cations, anions and substituents. For example, the water solubility of the ILs is influenced by the length of the alkyl chain (C_nH_{2n+1}). Increasing the length of the alkyl chain tends to decrease the water solubility by increasing the hydrophobicity of the cation [J.F. Brennecke et al, 2001). The imidazolium salts with halide, acetate, nitrate and trifluoroacetate anions are totally miscible with water but with hexafluorophosphate [PF_6^-] and [$(CF_3SO_2)_2SO_3^-$] are immiscible and that with tetrafluoroborate [BF_4^-] and [$CF3SO_3^-$] can be totally miscible or immiscible depending on the substituents on the cation [Sedden et. al, 2000].

The study of liquid/vapor interface the interplay of molecular and ionic interaction is important for the understanding of the interfacial structure and dynamics. The highly polar nature of ILs causes the surfaces of IL liquids to become highly ordered in comparison with the surface of many other types of organic liquids. These surfaces are still poorly understood. Gaining a quantitative understanding of the surface properties of ILs is of equal importance for the purpose of understanding catalytic reactions, electrolytic reactions, phase transfer into the IL and lubrication. Simulation calculation of dimethylimidazolium chloride at 400 and 450 K find an enhance density near the interface different from the behavior in molecular liquids [Lynden-Bell R.M., 2003]. According to atomistic simulation, the cations are oriented with their planes perpendicular to the

surface and their dipoles in the surface plane. No segregation of cations and anions is found in the surface plane. Experimental investigation shows that the dipole vector of the imidazolium cation is perpendicular to the surface plane [Sedden et. al., 2001].

One of the ultimate goals of this research is to understand how the surface structure of the imidazolium based ionic liquid varies with temperature. We use the Ellipsometric measurement to study the surface structure of the IL. We also study the spreading behavior of the imidazolium based ionic liquid in hard surface (Silicon wafer) via contact angle measurement.

CHAPTER 2 – Theory

In this chapter, I will discuss theory behind the Ellipsometry and contact angle measurement.

Ellipsometry

When a linearly polarized beam of light is reflected at an oblique incidence from a specularly reflecting surface its state of polarization changed due to change in surface energy. The properties of the reflecting surface can be studied by measuring the relative phase and relative amplitude change of the reflected orthogonal electric fields.

The two orthogonal electric fields represent the two orientation of the polarization. One p orientation, represents the electric field component parallel to the light's plane of incidence (i.e. perpendicular to the interface) and the other s orientation, represents the electric field component perpendicular to the plane of incidence. The electric field vector of a monochromatic unpolarized light wave will have components in both directions. With time, these components will travel through the p-s plane in an ellipse. The shape of the ellipse depends on two factors- one the magnitude of the p and s components and other the phase difference between the components. With no phase difference between the components the resulting electric field vector travels in a line and id called linearly polarized light. If the phase difference equals to quarter wavelength with equal in magnitude, the

field vectors travel in a circle and is called circularly polarized light. Otherwise the field vector is called elliptically polarized [Hecht, 2002].

If r_p and r_s are the amplitudes reflectivity for the p and s polarized light respectively then the ellipticity is defined as the complex ratio

$$\frac{r_p}{r_s} = \rho\, e^{i\Delta}$$

where Δ is the phase difference between p and s polarized components and ρ is the ellipticity. For a interface where Fresnel's equations are apply, ρ equals unity for normal incidence, goes to zero at the Brewster angle where Δ jumps discontinuously by π radians and raises to unity at grazing incidence for external reflection.

<u>Figure 2.1</u> Example of a right-handed (clockwise) polarization ellipse.

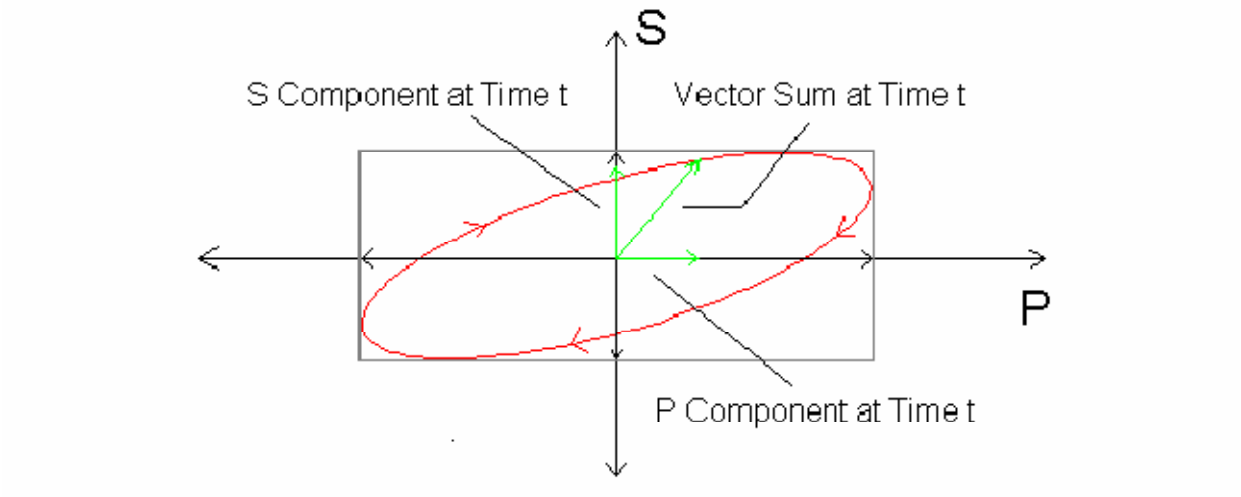

At Brewster angle of incidence (at which only s polarized light can reflect) the real part of the ratio vanishes and the remaining imaginary part is known as the coefficient of ellipticity ($\overline{\rho}$)

$$\bar{\rho} = \mathrm{Im}\left(\frac{r_p}{r_s}\right)\Big|\,\theta_B$$

For a step surface of zero thickness, $r_p = 0$, so. For a nonzero surface thickness $\bar{\rho}$ is nonzero. The advantage of measuring $\bar{\rho}$ at Brewster angle is that only surface effects contribute to the ellipticity.

Drude first found the relation between the coefficient of ellipticity and dielectric constant of a transition region where the dielectric constant varied only with depth as $\epsilon(z)$ between the bulk values ϵ_1 and ϵ_2 by correcting the Fresnel's equation

$$\bar{\rho} = \frac{\pi}{\lambda}\sqrt{\frac{\epsilon(+\infty)+\epsilon(-\infty)}{\epsilon(+\infty)-\epsilon(-\infty)}}\int_{-\infty}^{+\infty}\frac{[\epsilon(z)-\epsilon(+\infty)][\epsilon(z)-\epsilon(-\infty)]}{\epsilon(z)}\,dz$$

where $\epsilon(z)$ is the optical dielectric constant as a function of z, depth of the surface, and $\epsilon(-\infty)$ and $\epsilon(+\infty)$ are the optical dielectric constants of the bulk incident and reflecting media respectively. λ is the wavelength of the incident light [Beaglehole, 1980].

Contact Angle

The spreading of liquid droplets on solid surface is very important for the understanding of lubrication, molecular scale friction, and coating dynamics [P.G. de Gennes, 1985]. When the liquid droplet is brought into contact with the flat, smooth, and horizontal solid surface, the liquid's spread onto the solid as excess capillary potential energy is dissipated during the motion and depends on the

surface energy of the solid. Under classic conditions of wetting on a smooth, horizontal and hard solid the kinetics of spreading is controlled essentially by a dynamic energy balance between the rate of restitution of capillary potential energy and viscous dissipation occurring through shear motion within the liquid. The resulting shape of the liquid drop depends on the forces at the three interfaces. For a liquid drop on the solid substrate sitting in air, the interfaces are located at the solid-vapor boundary, the liquid-vapor boundary and the liquid-solid boundary. The forces are related by Young's equation

$$\sigma_{SV} = \sigma_{SL} + \sigma_{LV} \cos\theta \text{ ---------- (2.)}$$

where σ_{SV}, σ_{SL} and σ_{LV} are the energy per unit area at the solid-vapor, solid-liquid and liquid-vapor interfaces respectively. θ is the contact angle of the liquid on the solid. The contact angle measures the wetability of the surface i.e. how far the liquid drop spreads out on the surface. For the liquid with high surface energy

<u>Figure 2.2</u> Diagrams of the forces that determine contact angle.

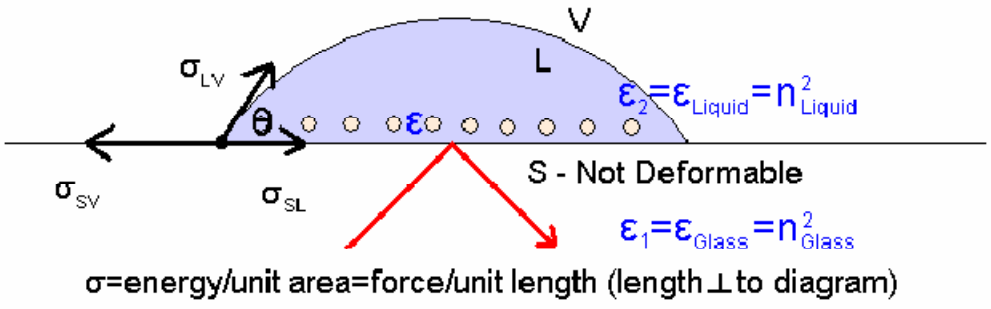

at the solid-liquid interface or the low surface tension of the solution's surface, the contact angle is small i.e. the drop spreads out over the surface. This surface is said to be wetable and is called hydrophilic. For the low surface energy, the drop 'balls

up' on the surface (high contact angle). The surface is said to be non-wetable and is called hydrophobic.

Figure 2.3 Examples of a slightly hydrophobic surface (L) and a hydrophilic surface (R).

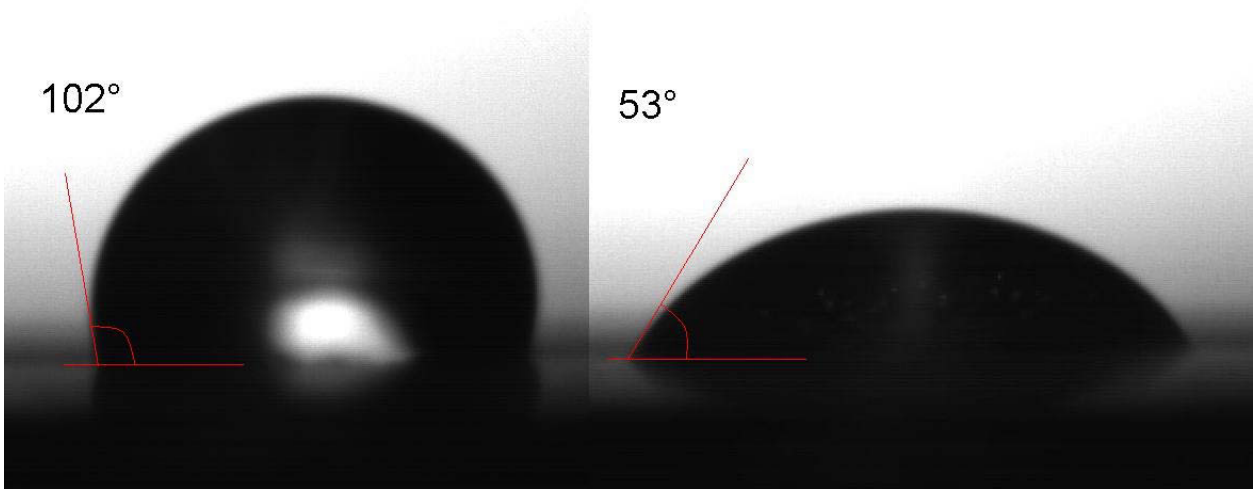

CHAPTER 3 – Apparatus

In this chapter, I will discuss the experimental set up for the Ellipsometric measurement and contact angle measurement.

Phase Modulated Ellipsometer

The optical scheme of the phase modulated Ellipsometer first designed by Dr. Bruce Law (Law, 1984) is shown in Figure 3.1. It consists of Laser, NF = neutral density filter, P = polarizer, BM = birefringence modulator, A = analyzer, I = iris, S = scatter plate and PMT = photomultiplier tube. The optical components are mounted in a vertical configuration in order for the light to reflect off a horizontal liquid surface. A 5mW He-Ne laser of wavelength λ=632.8nm is used as a light source. The intensity of the light is reduced to ~1% by the neutral density filters (NF) so that the detector can handle the output signal. The light is linearly polarized at 45^0 to the p and s direction at the polarizer (P). So that the field amplitudes along $\hat{s}$ and $\hat{p}$ directions are identical. The electric field that comes out from the polarizer is

$$\vec{E} = \frac{E_0}{2}(\hat{s} + \hat{p})$$

where E_0 is the total amplitude.

The phase of the light is modulated sinusodially at frequency $f_0 = \frac{\omega_0}{2\pi}$ ~ 50 kHz (Resonance frequency of the quartz crystal) by a high stability birefringence modulator (BM). The electric field vector after modulator becomes

$$\vec{E} = \frac{E_0}{\sqrt{2}} \left(\hat{s} + e^{i\delta_0 \sin \omega_0 t} \hat{p} \right)$$

where δ_0 and ω_0 are the amplitude and angular frequency of the phase shift. This is the signal which is incident on the sample surface. The sample is placed at the geometric center of the Ellipsometer so that the incident and reflected beam are

Figure 3.1 Optical arrangement of phase modulated ellipsometer.

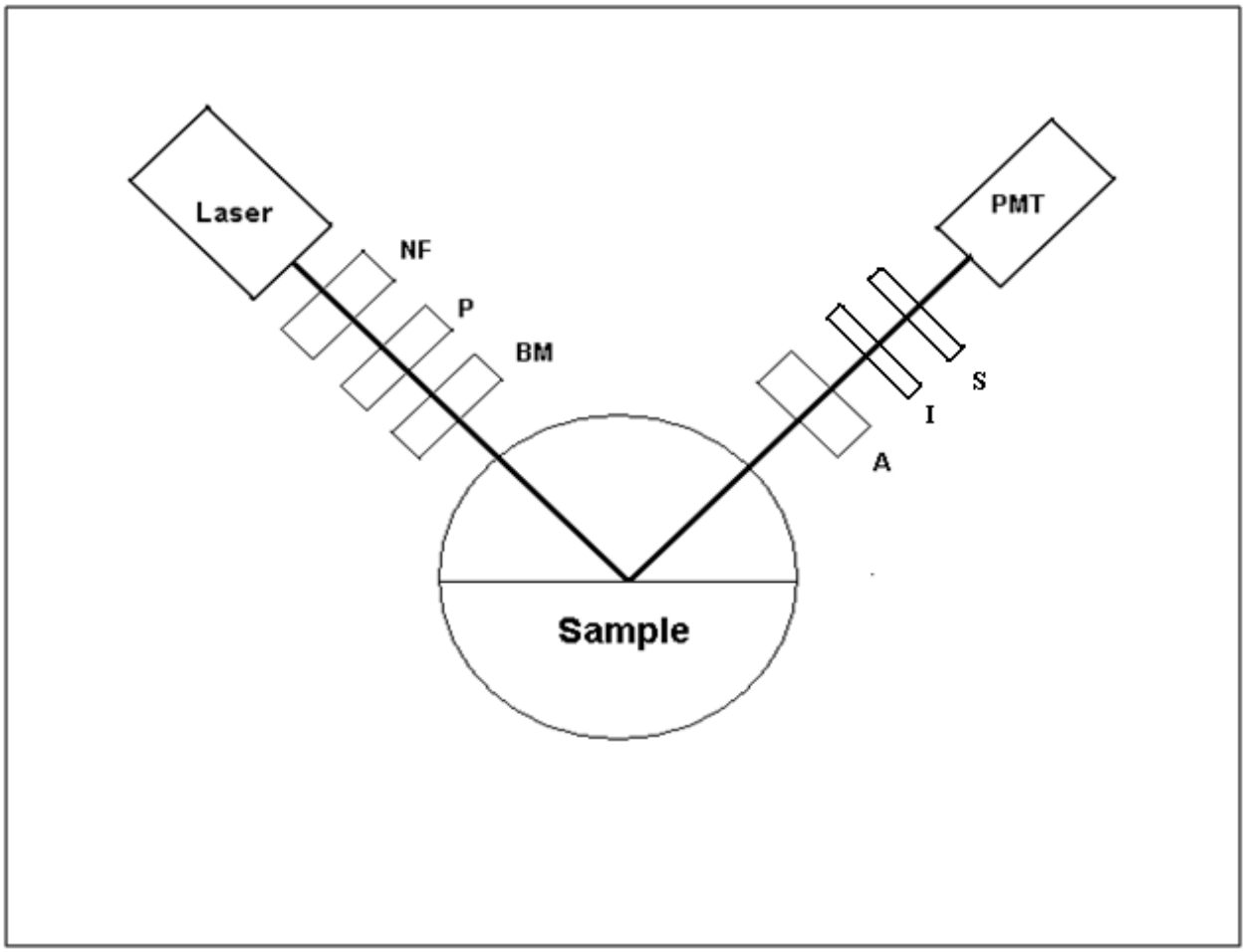

normally incident on the wall of the sample holder. The reflection at the liquid-vapor surface provides both the change in the amplitude and the phase of both the s and p polarizations. The reflected signal from the surface is described by

$$r_s = r_{s0}\, e^{i\delta_s}$$

and $$r_p = r_{p0} e^{i\delta_p}$$

So the electric field after reflection from the sample can be written as

$$\vec{E} = \frac{E_0}{\sqrt{2}} \left(r_{s0}\, e^{i\delta_s}\, \hat{s} + r_{p0} e^{i(\delta_p + \delta_0 \sin \omega_0 t)} \hat{p} \right)$$

The reflected signal is passed through the analyzer (A) which consists of two orthogonal pieces of Polaroid oriented at 45^0 to the s direction and driven at low frequency. The analyzer is capable of automatically rotating at $\pm 45^0$ relative to the s direction. So that the electric field amplitude between analyzer and photomultiplier tube is

$$\vec{E} = \frac{E_0}{2} \left(r_{s0}\, e^{i\delta_s}\, \hat{s} \pm r_{p0} e^{i(\delta_p + \delta_0 \sin \omega_0 t)} \hat{p} \right)$$

The photomultiplier tube (PMT) is used to collect the light reflected from the sample surface. The iris (I) shields the photomultiplier tube from the room light. A scatter plate consisting of a 1mm thick fused quartz slide is mounted at the front of the PMT to spread the light homogeneously over the cathode surface in order to eliminate the sensitivity of the PMT to the position of the beam. The PMT measures the intensity of the light and is given by

$$I \propto \left| \vec{E} \right|^2$$

$$= \frac{{E_0}^2}{4}\ {r_{s0}}^2\ [1 + \rho^2 \pm\ 2\rho\ \cos(\Delta + \delta_0 \sin\omega_0\, t)]$$

where $\rho = \frac{r_{s0}}{r_{p0}}$ and $\Delta = \delta_p - \delta_s$.

The cosines inside the square bracket can be expanded in terms of Bessel functions as

$$\cos(\Delta + \delta_0 \sin\omega_0\, t) = \cos\Delta\cos(\delta_0 \sin\omega_0\, t) - \sin\Delta\sin(\delta_0 \sin\omega_0\, t)$$

$$= \cos\Delta[J_0(\delta_0) + 2J_2(\delta_0)\cos 2\omega_0 + \ \ldots\ldots\ldots\ldots\ldots\ldots] -$$

$$\sin\Delta[2J_1(\delta_0)\sin\omega_0 t + 2J_3\,(\delta_0)\sin 3\omega_0\, t + \ \ldots\ldots\ldots\ldots.]$$

So

$$I = \frac{|E_0|^2}{4} {r_{s0}}^2[1 + \rho^2 \pm 2\rho\cos\Delta J_0(\delta_0) \pm 4\rho\cos\Delta\, J_2(\delta_0)\cos 2\omega_0\, t \pm$$

$$\ldots\ldots \mp \quad 4\rho\sin\Delta\, J_1(\delta_0)\sin\omega_0\, t \mp 4\rho\sin\Delta J_3(\delta_0)\sin 3\omega_0\, t \mp \ \ldots\ldots\ldots..]$$

$$= \frac{|E_0|^2}{4}\ \frac{{r_{s0}}^2}{1+\rho^2}\Big[1 \pm\ \frac{2\rho}{1+\rho^2}J_0(\delta_0)\cos\Delta \mp \frac{4\rho}{1+\rho^2}J_1(\delta_0)\sin\Delta\sin\omega_0 t \pm$$

$$\frac{4\rho}{1+\rho^2}J_2(\delta_0)\cos\Delta\cos 2\omega_0\, t \pm\ \ldots\Big]$$

$$= I_0[i_{dc} + i_{ac}(\omega_0) + i_{ac}(2\omega_o)]$$

where

$$I_0 = \frac{|E_0|^2}{4}\ \frac{{r_{s0}}^2}{1+\rho^2}$$

$$i_{dc} = 1 \pm \frac{2\rho}{1+\rho^2}\, J_0(\delta_0)\cos\Delta$$

$$i_{ac}(\omega_0) = \mp \frac{4\rho}{1+\rho^2}\, J_1(\delta_0)\sin\Delta\sin\omega_0\, t$$

$$i_{ac}(2\omega_0) = \pm \frac{4\rho}{1+\rho^2}\, J_2(\delta_0)\cos\Delta\cos 2\omega_0$$

The birefringence modulator allows for the adjustment of δ_0 so that $J_0(\delta_0) = 0$ at $\delta_0=0.765\pi$. The output signals are now measures with lock-in amplifier (LA) at the corresponding frequency keeping i_{dc} constant. The voltage signals detected by the LA are

$$V_{ac}(\omega_0) \cong \mp \frac{4\rho}{1+\rho^2} J_1(\delta_0) \sin \Delta$$

$$V_{ac}(2\omega_0) \cong \pm \frac{4\rho}{1+\rho^2} J_2(\delta_0) \cos \Delta$$

The values of $J_1(\delta_0)$ and $J_2(\delta_0)$ are found via calibration of the Ellipsometer. The quantities ρ and Δ provides the information about the sample surface.

Alignment and Calibration

All the optical components of the Ellipsometer are mounted on the rotatable arm, which is pivoted at the center of the optical table, so that the laser beam is parallel to the table. The laser, polarizer and the birefringence modulator are mounted on the left ellipsometer arm and the analyzer and the photomultiplier tube are mounted on the right arm (Figure 3.1). The arms are built to be moved together using a stepping motor and the computer controlled motor controller. The system is aligned in the following away:

First, the laser beam is aligned horizontally by removing each component of the ellipsometer so that the laser beam passes through the center of the photomultiplier tube.

Second, the polarizer is aligned in the absence of the analyzer and birefringence modulator. The s and p directions of the polarizer are found using reflection at the Brewster angle. The laser beam is made to reflect from the horizontal surface and the p axis of the polarizer is found for the minimum intensity of the reflected beam. The operating position of the polarizer is obtained rotating it by 45^0 relative to the p-axis.

Next, two directions i.e. parallel and perpendicular to the polarizer's operating orientation of the analyzer are found. For this the incident and reflected arms of the ellipsometer put horizontal with sample removed and determine the analyzer orientation which extinguish (no intensity) light when the polarizer is in its operating position and when it is rotated by 90^0 relative to its operating position.

At last, the birefringence modulator is aligned with its fast axis along the p-axis and the polarizer is in p-direction. The analyzer is oriented at $\pm 45^0$ to the p-axis. The correct position of the birefringence modulator is the position which minimizes the $V_{2\omega_0}$ i.e. at 2f the value of the voltage at phase 0^0 and 90^0 with fine tuning of the phase, then $J_0(\delta_0) = 0$. For the lock-in amplifier

$$V_{\omega_0} = 0 \qquad \text{for all } \theta$$

$$\text{And} \quad V_{2\omega_0} = 0 \qquad \text{for } \theta = 0$$

The calibration of ellipsometer is done by putting its arms horizontal with the polarizer is in 45^0 relative to its p-axis and analyzer is in $\pm 45^0$ with p-direction.

We have

$$i_{ac}(\omega_0) = \mp \frac{4\rho}{1+\rho^2} J_1(\delta_0) \sin\Delta \sin\omega_0 t$$

$$i_{ac}(2\omega_0) = \pm \frac{4\rho}{1+\rho^2} J_2(\delta_0) \cos\Delta \cos 2\omega_0$$

From these two equations it can be seen that

$$i_{ac}(\omega_0) = 0 \qquad \text{for } \Delta = 0$$

and $$i_{ac}(2\omega_0) = 0 \qquad \text{for } \Delta = \pi/2$$

For $\Delta = 0$, $2\omega_0$ signal becomes maximum which calibrates the $2\omega_0$ and $2V_0$. For $\Delta = \pi/2$, ω_0 signal becomes maximum and gives ω_0 and V_0 values.

For $2\omega_0$ calibration, switch the 2f button and adjust the phase on the lock-in until the resulting signal on the lock-in is zero. When the phase of the reference voltage is flip by 90^0 the resulting values give the phase and voltage i.e. 2f and $2\omega_0$.

For ω_0 calibration a quarter wave plate ($\Delta = \pi/2$) is inserted along the path of the laser beam and the reference setting change to f. Again adjust the phase on the lock-in until the voltage is zero then offset the by 90^0, the resulting readings are f phase and V_0 voltage.

Contact Angle Measurement

For the contact angle measurement we use the Long Range Microscope Kit. This kit is intended for viewing sessile drop and allowed the microscope to be placed a considerable distance from the drop. The light source (Cole-Parmer 41723, 150W) is placed behind a lab jack, on which lens tissue and a substrate coated slide is placed. A small needle head is held over the surface where the liquid drop will be applied, and the slide location and camera focus is adjusted until the head of the liquid drop is seen clearly. The surface used for spreading of liquid was silicon wafer. The FTA32 software is used to capture the video of the spreading of the liquid drop with time at one frame per second. This interval is short enough to observe the spreading of ionic liquid on hard surface. FTA32's recording is started and the liquid drop is applied to the substrate vertically. Once the liquid drop made contact with surface the FTA32 starts to measure the contact angle. The experiment is run until the liquid drop almost stop to spread. Once the experiment is complete, the FTA32 software is used to analyze each frame. By manual application of the surface line and a line of curvature, the program calculates contact angle, drop base width, volume, and other parameters. The shape of the liquid drop seen from the camera at any time is shown in figure 3.2. The shape of the liquid drop changes with time which becomes more flat and flat as time goes on.

<u>Figure 3.2</u> Shape of the liquid drop observed from camera at certain time.

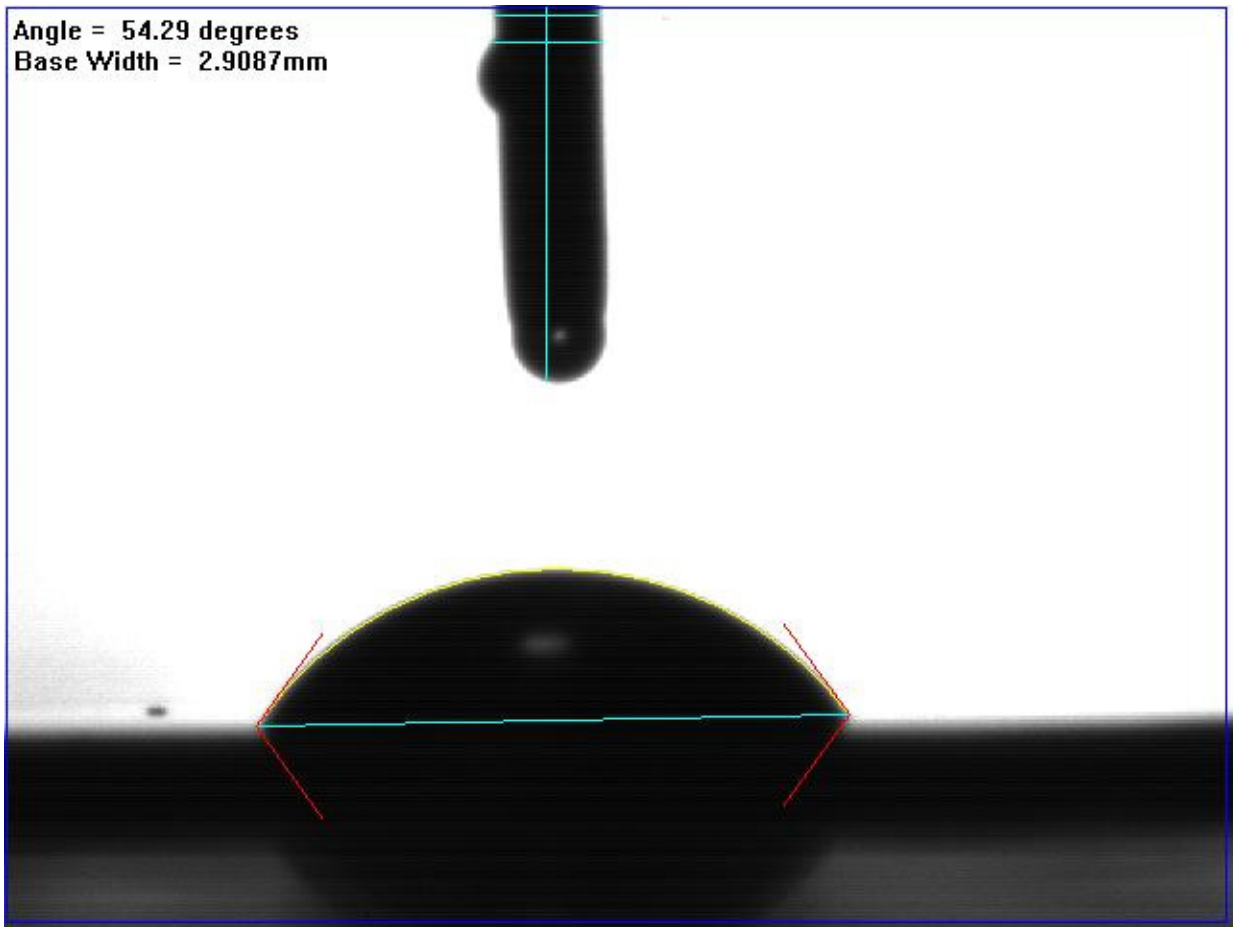

CHAPTER 4 - Result and Analysis

Ellipsometric Measurement

For the Ellipsometric measurement we use ionic liquid 1-Ethyl-3-methylimidazolium hexafluorophosphate ($C_6H_{11}F_6N_2P$). The melting of this ionic liquid is ~60^oC. The structure of this ionic liquid is shown in figure 4.1. The Ellipsometric measurements were done above the melting point of the ionic liquid using phase modulated ellipsometer described in Chapter 3 to understand the surface orientational order of the dipole moment. A glass container is used to put

<u>Figure 4.1</u> Structure of 1-Ethyl-3-metyl imidazolium hexafluorophosphate

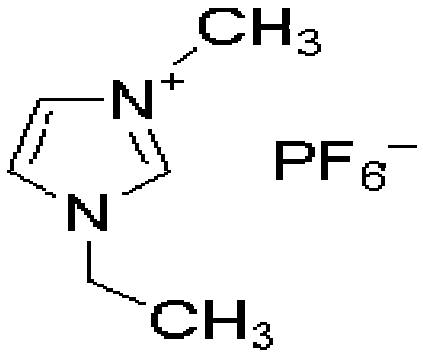

the ionic liquid. The glass container is first sonicated in acetone, ethanol and toluene for 5 minutes and after each sonication it is dried by hot air gun. Then the glass container is cleaned by the glass etch (mixture of equal amount of distill water and HNO_3 and 5% of HF of either water or HNO_3). After glass etch the glass

container is cleaned by Millipore water and put in the oven to dry out for 24 hours. The ionic liquid initially in powder form put on the cleaned glass container and heated until it melts and then cooled down to solidify it. The sample ionic liquid is now placed at the center of the oven having glass window through which light can pass and aligned in such way that the light reflected from the sample pass through the center of the photomultiplier tube. The temperature of the oven is controlled by Lakeshore. The experiment is run at the Brewster angle (i.e. fixed angle) and data were taken at each set temperature. I ran the experiment two times; one inside the oven without using vacuum and other inside the same kind of oven using vacuum. The variation of ellipticity for both the experiment is shown in figure 4.3. From the figure it is seen that the imaginary part of the ellipticity increases gradually with increase in temperature up to 385 K in the first experiment. Its magnitude drops at temperature 385 K suddenly and remains almost constant on further increase in temperature. But for the second experiment it is seen that the imaginary part of the ellipticity almost remains constant with increase in temperature up to 385 K. Then as the temperature increases further imaginary part decreases and remains almost constant on further increase in temperature. The discrepancy on the result for two experiments may due to use of vacuum. In the first experiment I saw there is some condensation on the glass window which might change the properties of the reflected light from the surface of the liquid. But for both the case, it can be seen that there is some discontinuity in the imaginary part at temperature 385 K.

<u>Figure 4.2</u> Variation of imaginary part of the ellipticity of 1-Ethyl-3-methylimidazolium hexafluorophosphate.

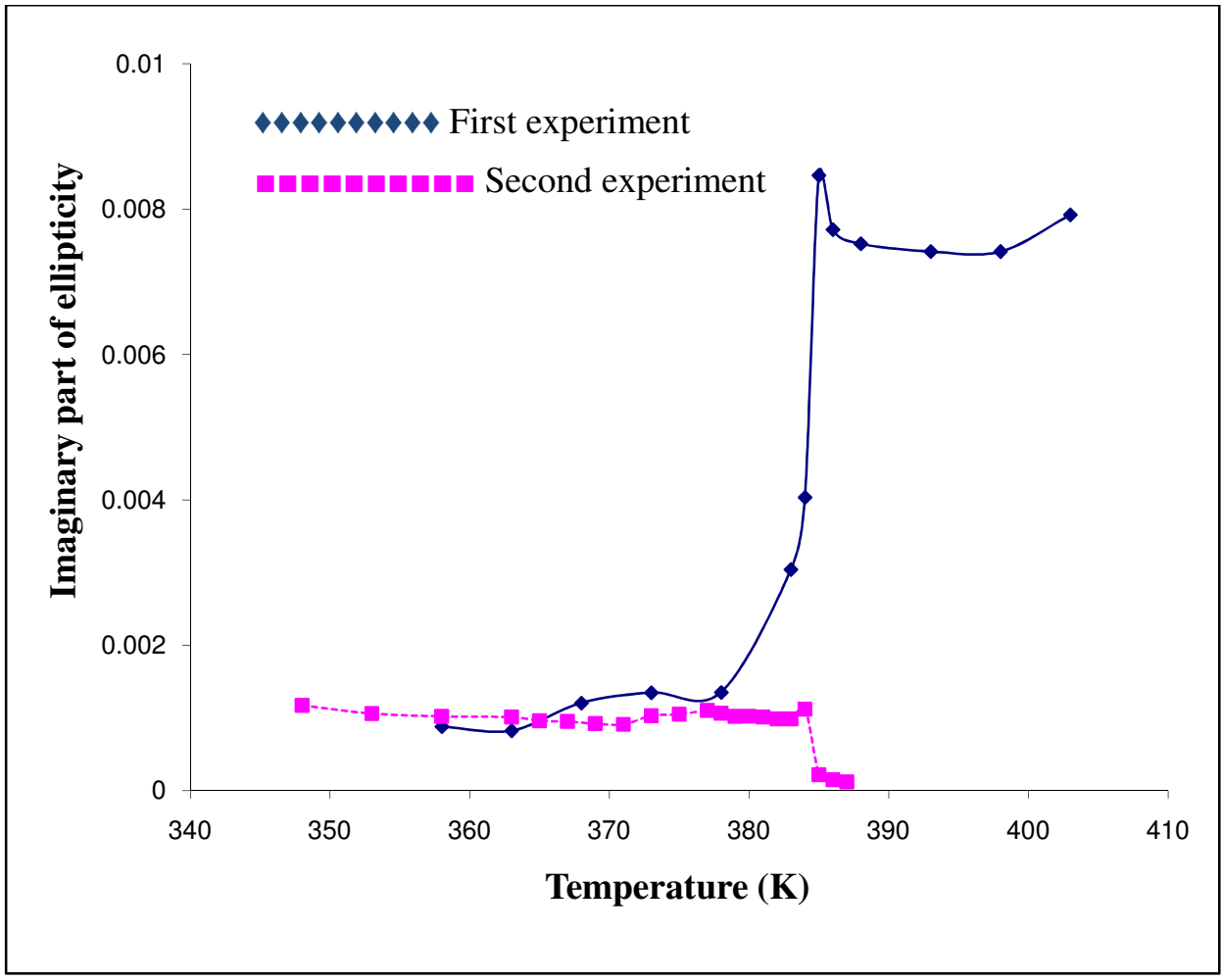

I also plot the variation of real part of the ellipticity with temperature for both the experiment. The plot is as shown in figure 4.3. Since the experiment is done at Brewster angle the initial real values are very close to zero. From the graph it is seen that the real part of the ellipticity first decrease gradually as the temperature increases. At temperature 385 K the real part increases and then remains almost

constant on further increase in temperature. In real part also, there is difference in magnitude for the two experiments. But it is important to see that for both the experiment and for both the real and imaginary part the ionic liquid posses some transition at temperature 385 K.

<u>Figure 4.3</u> Variation of real part of the ellipticity of 1-Ethyl-3-methylimidazolium hexafluorophosphate.

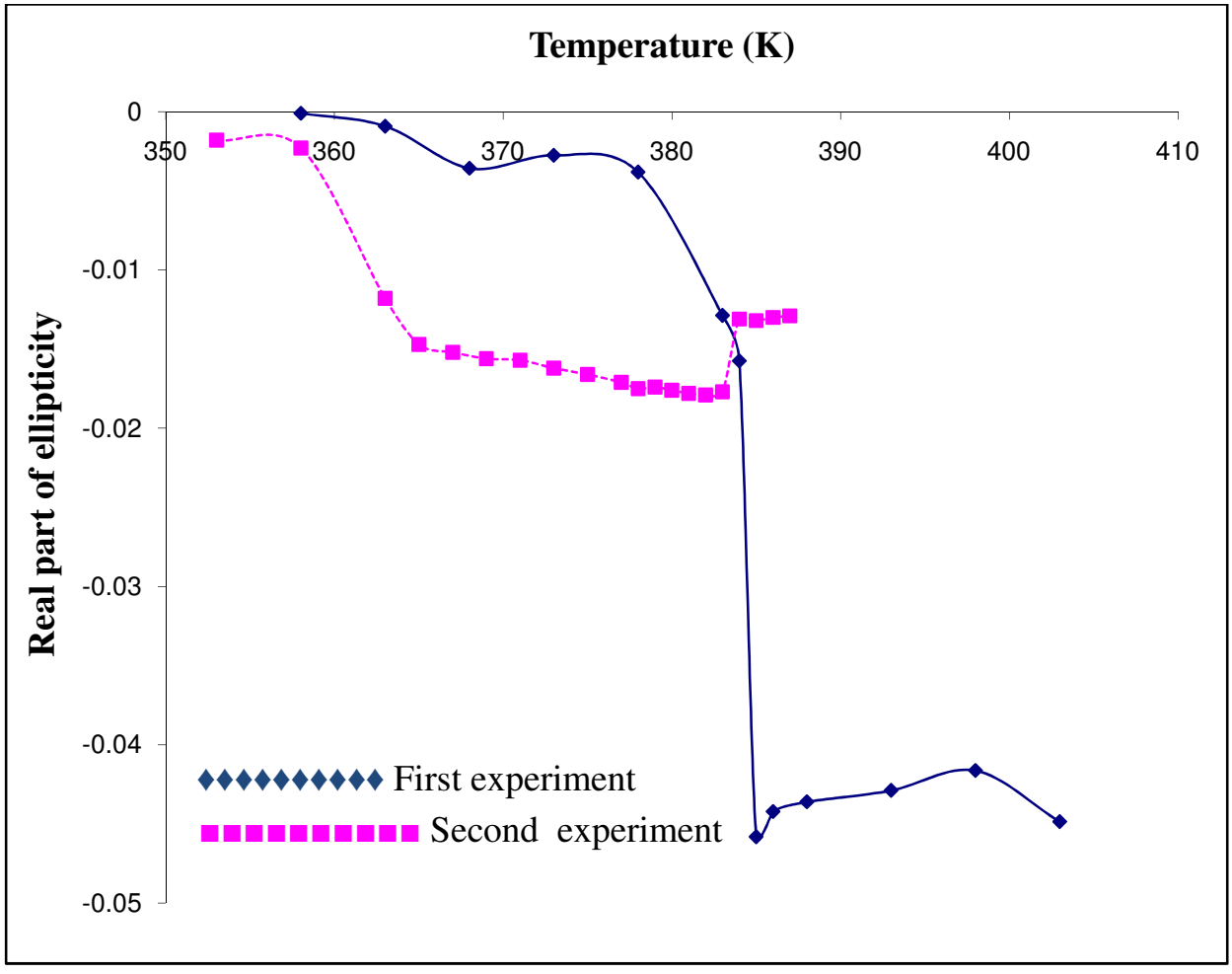

Similar kind of behavior was found for the surface dipole moment density of the $[C_4mim]^+PF_6^-$ liquid/vapor interface with temperature, shown in figure 4.4 [Freyland et.al, 2005]. They assume that this is indicative of a first order ferroelectric phase transition at temperature 385 K. This can be described by an interfacial order-disorder transition with a critical temperature of T_c=385 K. The observed values of the ellipticity from the ellipsometer are given in table 4.1 for the first experiment and in table 4.2 for the second experiment.

Temperature(K)	Imaginary part of the Ellipticity	Real part of the Ellipticity
358	0.000878	-0.00011
363	0.000823	-0.00092
368	0.001203	-0.00358
373	0.001346	-0.00276
378	0.001351	-0.00382
383	0.003043	-0.001287
384	0.004034	-0.01575
385	0.008467	-0.04582
386	0.00772	-0.04422
388	0.007523	-0.04288
393	0.007417	-0.04162
398	0.004717	-0.04162
403	0.007921	-0.04485

<u>Table 4.1</u> Observed data for the second experiment without using vacuum.

Temperature (K)	Imaginary part of the Ellipticity	Real part of the Ellipticity
348	0.001171	-0.0014
353	0.00106	-0.0018
358	0.001021	-0.0023
363	0.00101	-0.0118
365	0.00096	-0.0147
367	0.00095	-0.0152
369	0.00092	-0.0156
371	0.00103	-0.0162
373	0.00105	-0.0166
375	0.0011	-0.0171
377	0.001062	-0.0175
379	0.00102	-0.0174
380	0.001022	-0.0176
381	0.00101	-0.0178
382	0.000987	-0.0179
383	0.000987	-0.0177
384	0.000112	-0.0131
385	0.00022	-0.0132
386	0.00015	-0.013
387	0.00012	-0.0129

Table 4.2 Observed data for the first observation with using vacuum.

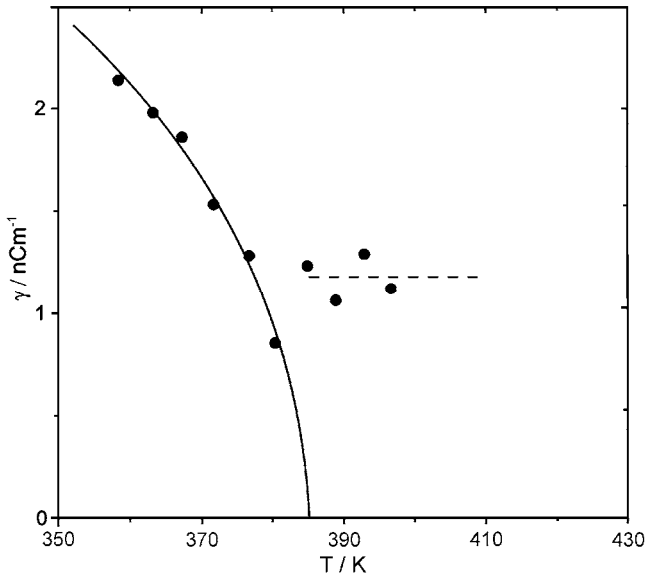

Figure 4.4 Temperature dependence of the surface dipole moment density of the $[C_4mim]^+PF_6$ liquid/vapor interface. The solid line corresponds to the fit of $\gamma/\gamma_0 = \tanh (T_c \gamma/ \gamma_0 T)$, where $\gamma_0 = 4.95$ nCm^{-1}.

Contact Angle Measurement

Different kinds of imidazolium based ionic liquids are used to study the spreading of the ionic liquid on the hard surface. The ionic liquids used are 1-Ethyl-3-methylimidazolium tetrafluoroborate of melting point ~ 15^{o}C and 1-Butyl-3-methylimidazolium tetrafluoroborate of melting point -71^{o}C. The structure of these ionic liquids is shown in figure 4.5. Since it is in liquid form at room temperature we use the camera/microscope system as described in Chapter 3, to measure the contact angle, in open air environment. As the ionic liquid is hygroscopic in nature

<u>Figure 4.5</u> Structure of 1-Ethyl-3-metyl imidazolium tetrafluoroborate (a) and 1-Butyl-3-methylimidazolium tetrafluoroborate (b).

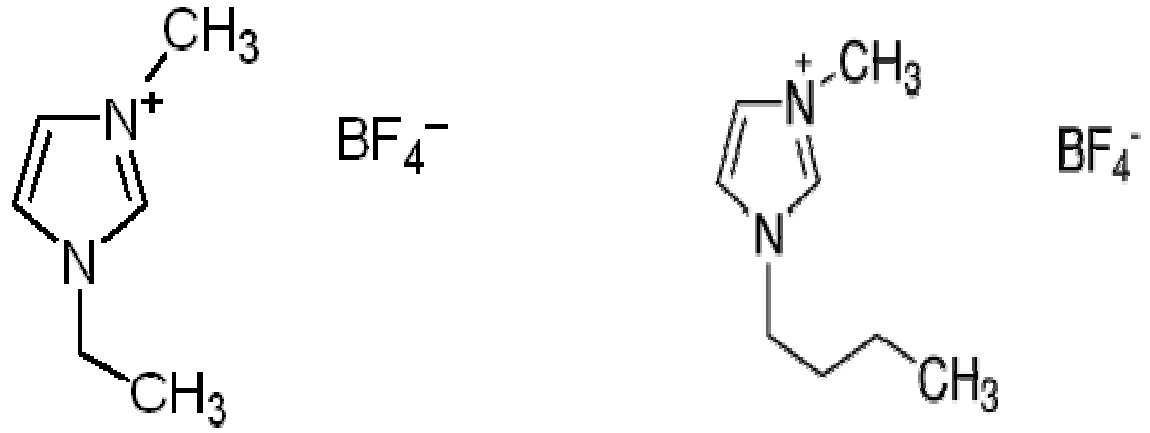

i.e. can absorb water vapor from the atmosphere which may cause the increase in the volume of the liquid drop. For our experiment we did not consider the water absorption and also the ionic liquid are non-volatile we assume the volume of the liquid drop is constant throughout the experiment. The FTA32 software is run for about 10 minutes after which the liquid drop comes in equilibrium position i.e. there is no further spreading.

The variation of the contact angle and base with time for 1-Ethyl-3-methylimidazolium tetrafluoroborate is shown in figure 4.6. It is clearly seen that there is definite change in the contact angle over the observation period. It was observed that the first few minutes the contact angle fell down rapidly then slowed down in later minutes and takes almost 10 minutes to come in equilibrium position

with equilibrium contact angle ~42^0. Similar kind of behavior was seen in the base radius also; first the base radius of the drop spread out rapidly and then slowed in the later minutes. The base area of the drop is an indicator of the surface energy and thus changing in base area with time represents the change in surface energy during the spreading of the liquid. Same kind of variation of contact angle and base with is found for the 1-Butyl-3-methylimidazolium tetrafluoroborate. The plot of contact angle and base with time for the 1-Butyl-3-methylimidazolium tetrafluoroborate is shown in figure 4.7 with equilibrium contact angle ~ 48^0.

<u>Figure 4.6</u> Variation of contact angle and base width vs. time for the ionic liquid 1-ethyl-3-methyl imidazolium tetrafluoroborate.

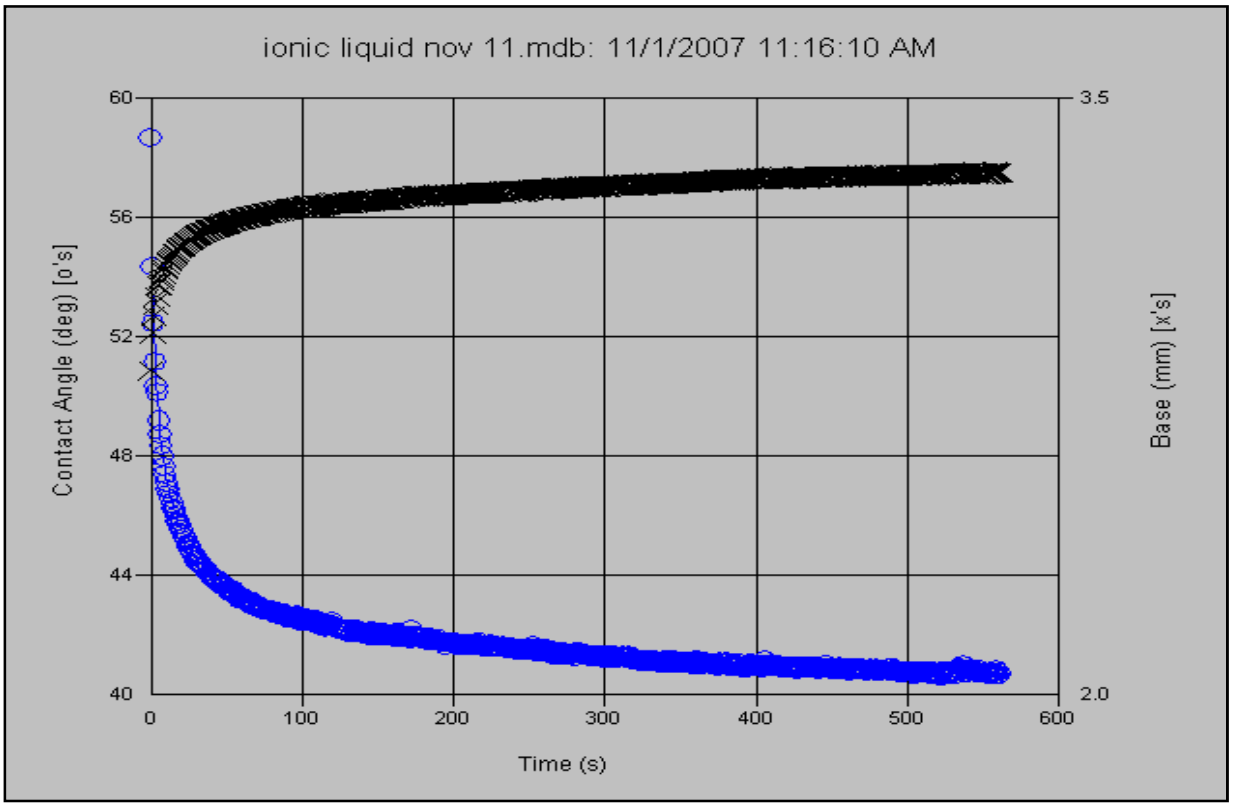

There is a driving force which is responsible for the spreading of the liquid drop on the surface. The driving force per unit length of the contact line is given by

$$F = \sigma_{LV} (\cos\theta_e - \cos\theta) * U$$

where σ_{LV} is the liquid-vapor surface tension, θ is the contact angle at any time, θ_e is the equilibrium contact angle and U is the contact line speed. The spreading of

<u>Figure 4.7</u> Variation of contact angle and base width vs. time for the ionic liquid 1-Butyl-3-methyl imidazolium tetrafluoroborate.

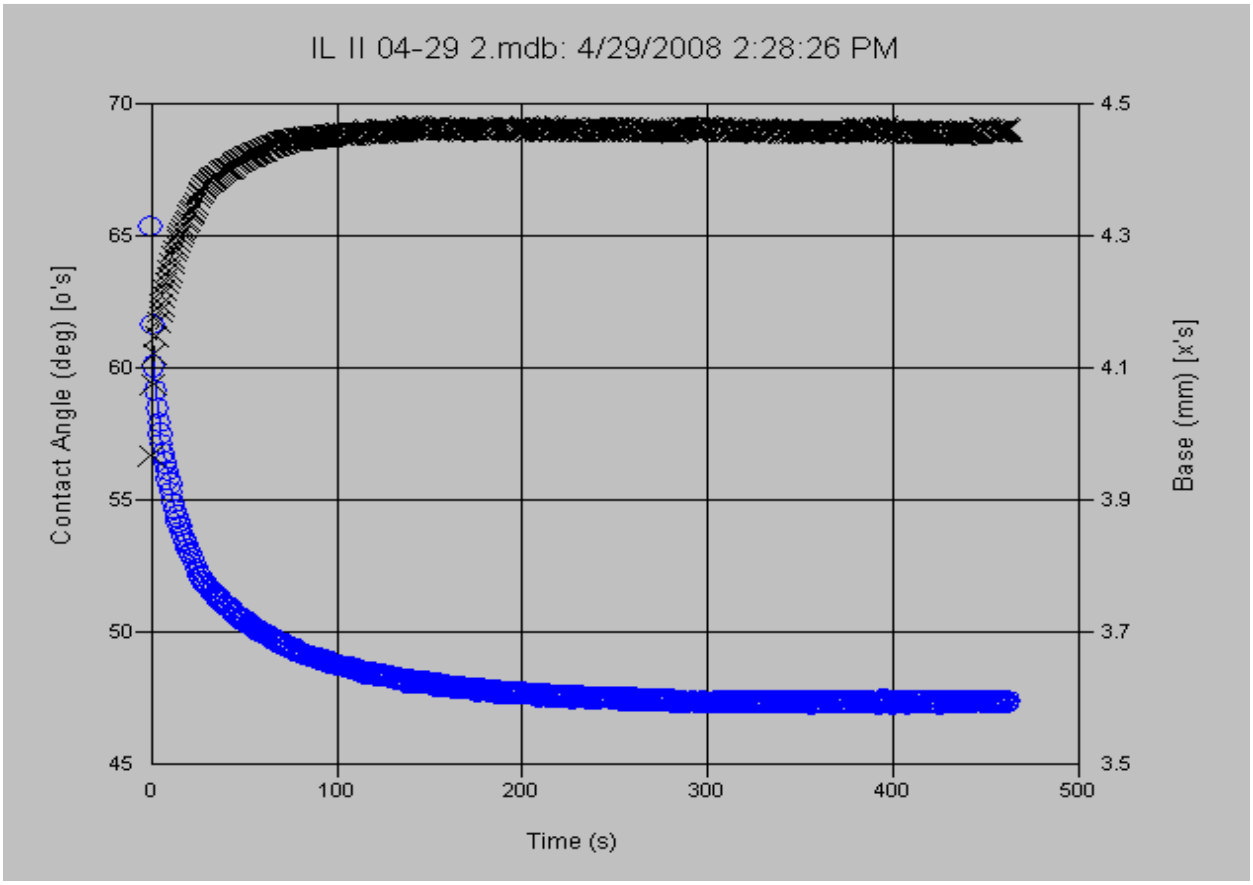

the liquid drop on any surface depends on the variation of the driving force per unit length with velocity. This driving force per unit contact length varies according to

the surface where the liquid drop is placed and the type of liquid used. For a normal liquid in hard surface the driving force varies as

in hydrodynamic regime $F \sim U^2\eta/\theta$

in kinetic regime $F \sim U \sin^{-1}\theta$

To observe the variation of the driving force per unit length we plot the graph between logarithm of (σ_{LV} ($\cos\theta_e$ - $\cos\theta$)* U) and U. The plot is as shown if figure 4.8. It is seen from the graph that the slope of the curve is 1.54. This means that the driving force varies as $U^{1.54}$. From this it is seen that the spreading of the ionic liquid on hard surface is different than that of the normal liquid which varies as U^2.

<u>Figure 4.8</u> Variation of driving force with speed of 1-ethyl-3-methyl imidazolium tetrafluoroborate.

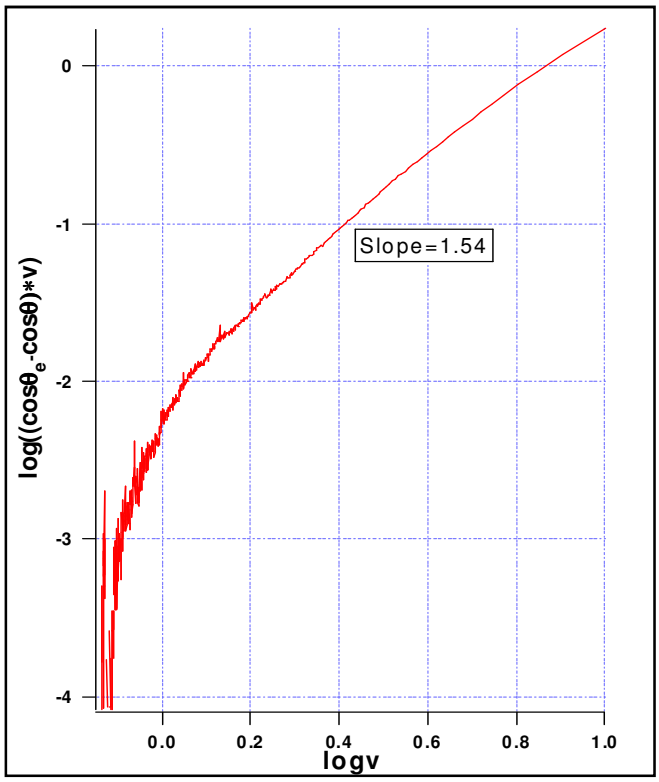

To make sure that the ionic liquid has different kind of spreading behavior on the hard surface we plot the graph between the logarithm of base radius and the time of spreading. The graph is shown in figure 4.9. From the graph it is seen that the slope of line is 0.023 suggesting that the base radius varies as $t^{0.023}$. But for the normal liquid the base radius varies as $t^{0.1}$. From these two graph it is clear that the ionic liquid definitely posses different spreading behavior than the normal liquid.

<u>Figure 4.9</u> Variation of base radius with time of 1-ethyl-3-methyl imidazolium tetrafluoroborate.

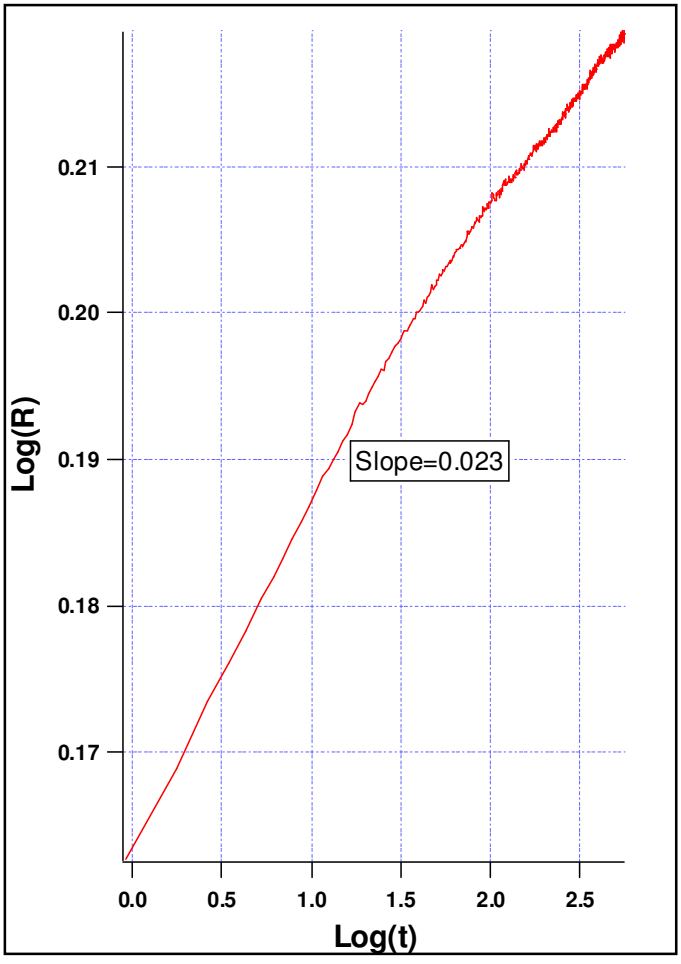

For the other ionic liquid 1-Butyl-3-methylimidazolium tetrafluoroborate, the variation of driving force with speed and base with time in logarithmic form is shown in figure 4.10. We observed that for both the ILs the slope for both the cases are almost same suggesting that the ILs posses a unique spreading behavior on the hard surface.

<u>Figure 4.10</u> Variation of driving force with speed (a) and base with time (b) of 1-ethyl-3-methyl imidazolium tetrafluoroborate.

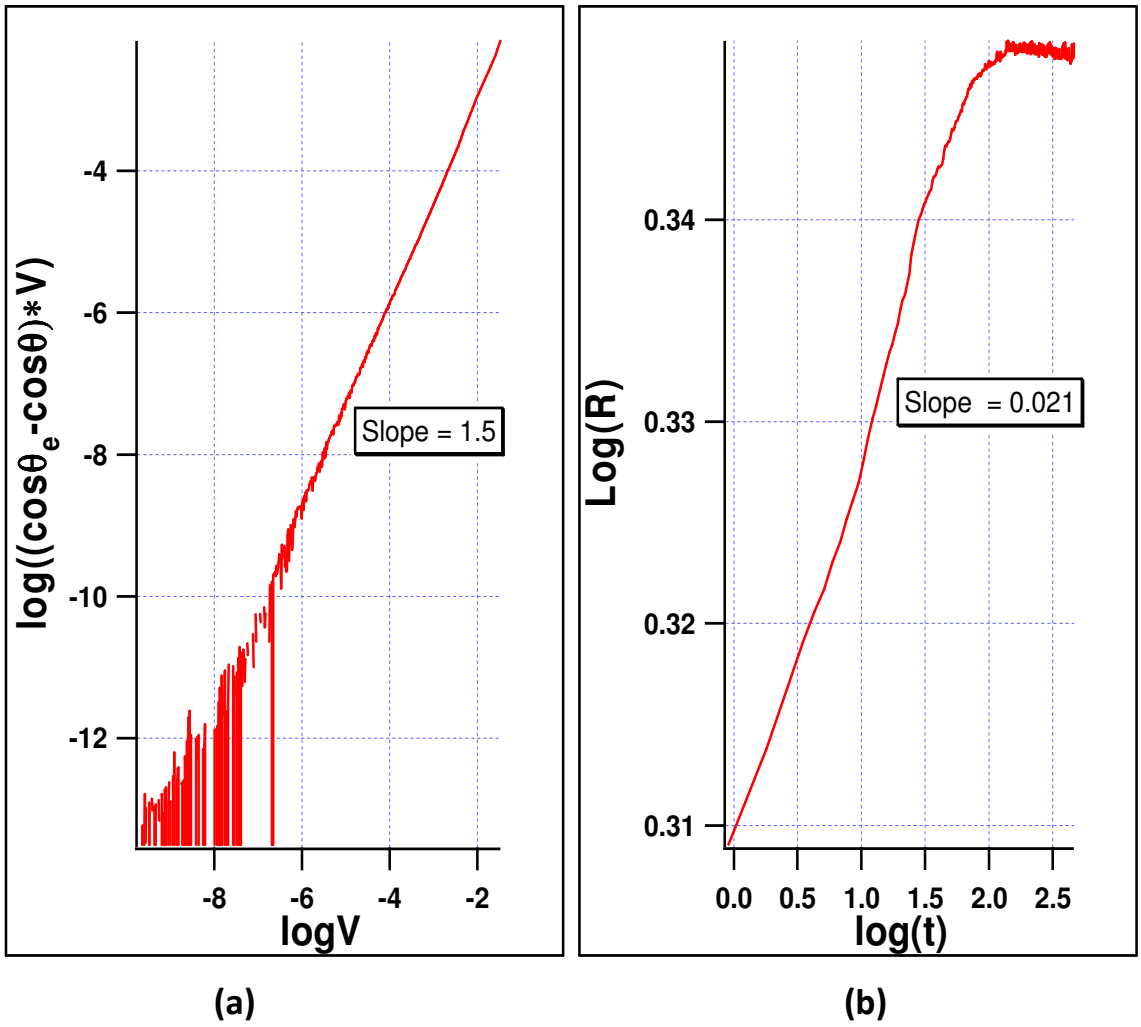

To make sure our system of measuring contact angle is right we try to observe the spreading of normal liquid on hard surface. We take a normal liquid Polydithylmethyl Siloaxne and observe the variation of contact angle with time on surface silicon wafer. The graph of contact angle vs. time is shown in figure 4.11.

Figure 4.11 Contact angle vs. time for Polydithylmethyl Siloaxne on Silicon wafer.

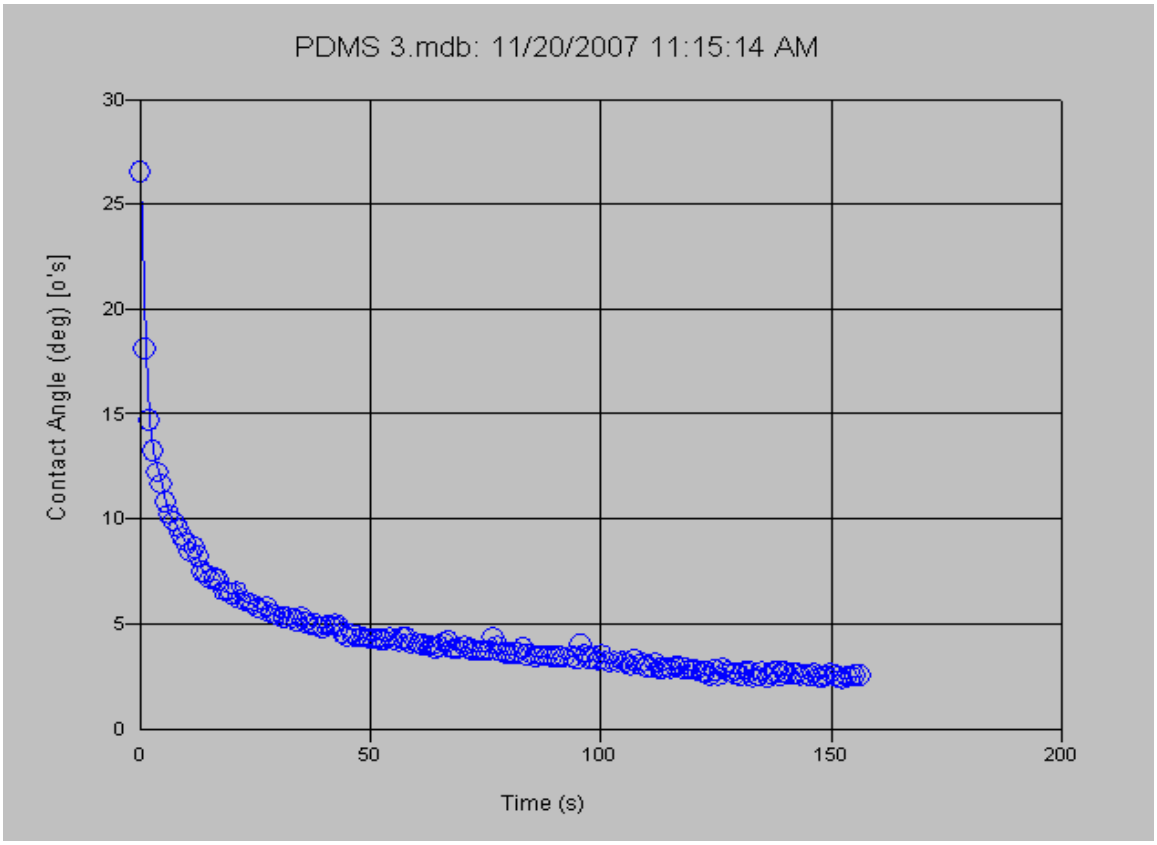

Since the equilibrium contact angle of the liquid is quite low, it is difficult to analyze the data. So to increase the equilibrium contact angle we use another hard surface HTS and measure the contact angle with time. The graph is shown in figure 4.12. From graph it is seen that the equilibrium contact angle increases remarkably.

<u>Figure 4.12</u> Contact angle vs. time for Polydithylmethyl Siloaxne on HTS.

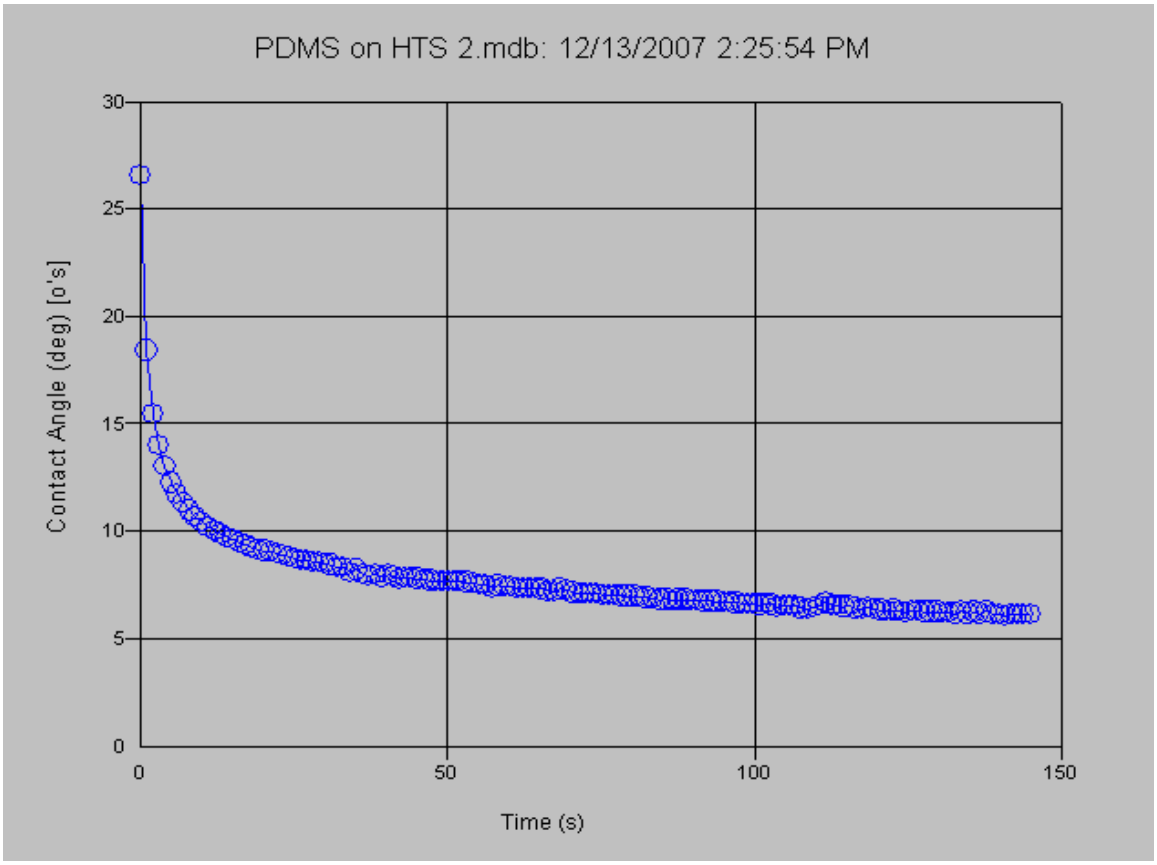

To compare with the result for the ionic liquid, we plot the graph between logarithms of base radius and time for the Polydithylmethyl Siloaxne. The graph is shown in figure 4.13. The slope of the base radius with time for the Polydithylmethyl Siloaxne is 0.095 i.e. the base radius varies as $t^{0.095}$. From the earliest work it was observed that the base radius varies as $t^{0.1}$ [Tanner, 1979]. This concludes that the system you are using to measure the contact angle is right. The different in slope of the curve of driving force vs. velocity and base radius vs. time conclude that the ILs have unique spreading behavior on the hard surface than that

of the normal liquid as PDMS liquid. To understand the theory behind this unique behavior of ILs other people in Dr. Law's group is also working on it. **<u>Figure 4.13</u> Comparison of variation of radius with time for ionic liquid and normal liquid. Lower for the ionic liquid and upper for the Polydithylmethyl Siloaxne.**

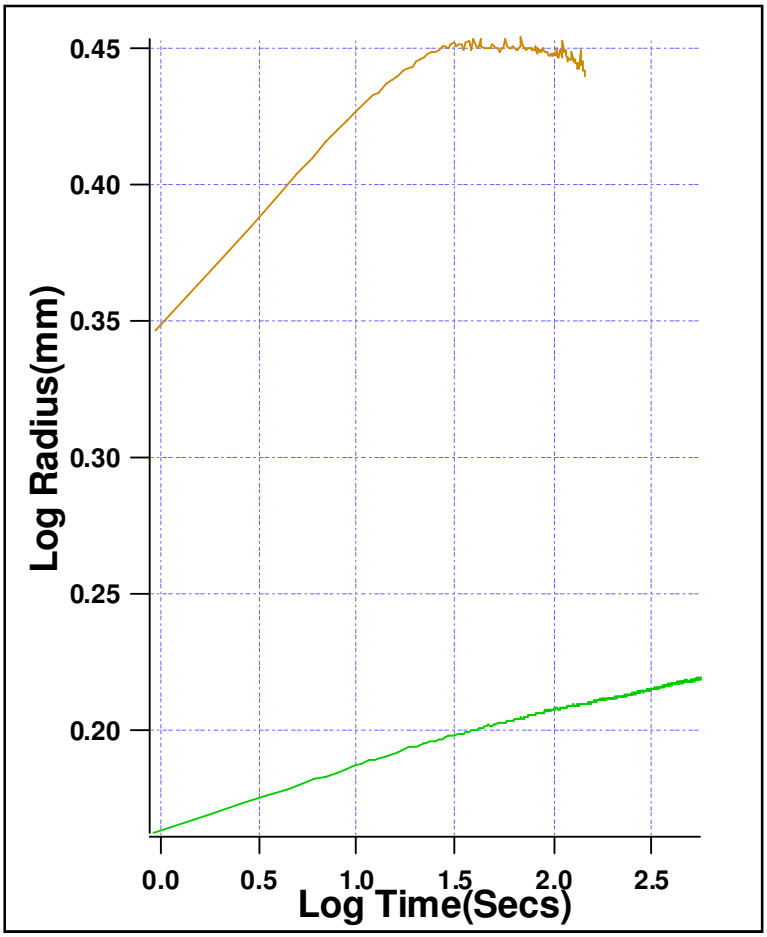

CHAPTER 5 –Discussion and Experimental Extension

The unique properties of ionic liquids (ILs), and the ability to tailor properties by choice of cations, anions, and substituents, offer the opportunities for the scientists to many more processing options than have available to us using conventional organic solvents.

The preliminary results reported here show that there is an order-disorder transition of dipole moment of imidazolium based ionic liquid at critical temperature of T_c= 385 K. To understand more about the orientation of dipole moment and surface structure of the ionic liquid one can extend this work by studying the zeolitic structures formed around micelle surface aggregates. Also, since the ellipsometry is most sensitive to long-range surface structure so to study the most resolving interfacial structure one can use the X-ray/neutron reflectometry which is most sensitive to short-range surface structure.

The contact angle measurement of imidazolium based ionic liquid on the hard surface (Silicon wafer) indicates that the ionic nature of the ILs plays an important role for the spreading. To understand more about the spreading of ILs on hard surface one can use other kind of ILs and other different hard surface such as HTS coated surface.

References

B.M. Law, "Properties of Interfaces", Doctoral Thesis, Victoria University of Wellington (1984).

D. Beaglehole, "Ellipsometric study of surface of simple liquids", Physica B 100, 163 (1980).

E. Hecht, Optics, 4th ed., Addison Wesley, San Francisco, 698 p (2002).

J. L. Anthony, E. J. Maginn and J. F. Brennecke, "Solution thermodynamics of imidazolium-based ionic liquid solution", J. Phys. Chem. B 105, 10942 (2001).

George Law, Philip R. Watson, Adrian J. Carmichael and Kenneth R. Sedden, "Molecular composition and orientation at the surface of room-temperature ionic liquids: Effect of molecular structure", Phys. Chem. Chem. Phys., 3, 2879 (2001).

K. R. Sedden, In Molten Salt Forum: Proceedings of 5th International Conference on Molten Salt Chemistry and Technology, Vol. 5-6, H. Wendt (Ed.), 53 (1998).

K. R. Sedden, A. Stark, and M. J. Torres, "Influence of chloride, water, and organic solvents on the physical properties of ionic liquids", Pure Appl. Chem., 72, 2275 (2000).

L. H. Tanner, "The spreading of silicon oil drops on horizontal surfaces", J. Phys. D: 12, 1473 (1976).

P. G. de Gennes, “Wetting: statics and dynamics”, Rev. Mod. Phys.Vol. 57, 827 (1985).

R.M. Lynden-Bell, “Gas-liquid interfaces of room temperature ionic liquids”, Mol. Phys. 101, 2625 (2003).

V. Halka, R. Tsekov and W. Freyland, “Interfacial phase transition in imidazolium-based ionic liquids”, J. Phys.: Condens. Matter 17 S3325 (2005).